Chemical Science

ROYAL SOCIETY OF CHEMISTRY

EDGE ARTICLE

View Article Online
View Journal

Check for updates

Cite this: DOI: 10.1039/d6sc02228f

All publication charges for this article have been paid for by the Royal Society of Chemistry

A unified cobalt-electrocatalytic platform for enantio- and stereo-selective C–H and C–F functionalization of *gem*-difluoromethylene allenes

Jiating Cai,†[a] Xinyu Gao,†[a] Chuitian Wang,†[a] Yang Li,†[a] Xiaoxin Tong,[a] Linzai Li,[a] Shi Qin,[a] Mingkai Yang,[a] Qixin Li,[a] Wei Wei,[a] Lei Ma,[a] Mei Wang,*[a] Si-Yan Liao,[a] Yugang Huang,[a] Xin Zhao,[a] Shengdong Wang,[a] Zhi Zhou,[a] Hui Gao,[b] Wei Yi*[a] and Zhongyi Zeng*[a]

While the merger of electrochemistry with enantioselective C–H functionalization has opened new avenues for assembling valuable chiral architectures, the simultaneous cleavage of strong C–H and C–F bonds *via* asymmetric electrocatalysis has remained elusive. Here, we present a unified electrochemical cobalt-catalyzed strategy that enables tandem enantioselective and stereoselective C–H and C–F functionalization with *gem*-difluoromethylene allenes, paired with hydrogen evolution. This resource-economic approach provides efficient access to a diverse range of enantiopure (*Z*)-fluoroalkenyl N-heterocycles bearing phosphorus-centered, axial, planar, and inherent chirality. Integrated experimental and computational mechanistic studies collectively support an unconventional Co(III/I/III/I) catalytic cycle, proceeding *via* sequential C(sp^2)–H metalation, allene insertion, reductive elimination, C(sp^3)–H metalation, alkene isomerization, and β–F elimination.

Received 18th March 2026
Accepted 9th May 2026

DOI: 10.1039/d6sc02228f

rsc.li/chemical-science

Open Access Article. Published on 11 May 2026. Downloaded on 6/1/2026 7:58:46 PM. This article is licensed under a Creative Commons Attribution-NonCommercial 3.0 Unported Licence.

Introduction

Merging electrosynthesis and asymmetric transition-metal catalysis has emerged as a powerful and sustainable platform for constructing chiral molecules.[1–10] This strategy uses electrical current to manipulate catalyst redox states, eliminating the need for stoichiometric sacrificial oxidants or reductants. Within this field, electrochemical enantioselective C–H functionalization is particularly attractive, as it enables the rapid assembly of high-value enantioenriched architectures and allows for late-stage diversification of complex structures, paired with hydrogen evolution as a benign byproduct.[11–14]

Electrochemical enantioselective C–H activation was pioneered by Ackermann *et al.* in 2020 for palladium-catalyzed asymmetric alkenylation/allylation[15–17] and annulation,[18] and was later extended to rhodium catalysis for enantioselective C–H annulation[19–21] and indolization (Scheme 1A).[22] The high cost and potential supply constraints of these noble metals, however, have driven the search for earth-abundant 3d transition-metal alternatives. Among them, cobalt stands as the most promising candidate, especially when combined with a chiral salicyloxazoline (Salox) ligand to form a versatile catalytic system.[23,24] This system has enabled electrochemical asymmetric C–H annulation,[25–36] esterification,[37–39] and etherification,[40] which typically proceed *via* Co(III/I) or Co(III/IV/II) catalytic manifolds.

Building upon our prior work on C–H/C–F dual functionalization with *gem*-difluoromethylene allenes (Scheme 1B),[41,42] and inspired by electrochemical cobalt/Salox-catalyzed asymmetric C–H activation with allenes,[29,31,34] we envisioned this cobalt-electrocatalytic system capable of enantioselective cleavage and functionalization of C–H and C–F bonds using *gem*-difluoromethylene allenes. A successful implementation would represent the first example of electrocatalytic asymmetric C–H/C–F functionalization.[43] However, its realization faced several fundamental mechanistic challenges: (a) the propensity of octahedral Co(III) species to adopt intricate coordination geometries, resulting in geometric and stereoisomerism; (b) complex reaction pathways involving multiple cobalt oxidation and spin states, further complicated by the fluoride anion byproduct; (c) the smaller atomic radius of Co(III), which impedes β–F elimination; (d) a potent hard acid/hard base interaction between the Co(III) center and fluoride that may suppress the dissociation of Co–F bond—a step essential for

[a]*Guangzhou Municipal and Guangdong Provincial Key Laboratory of Molecular Target & Clinical Pharmacology, The NMPA and State Key Laboratory of Respiratory Disease, School of Pharmaceutical Sciences, Guangzhou Medical University, Guangzhou, Guangdong 511436, China. E-mail: wangm0529@163.com; yiwei@gzhmu.edu.cn; zzeng@gzhmu.edu.cn*

[b]*School of Traditional Chinese Medicine and Health, Nanfang College Guangzhou, Guangzhou, Guangdong 510970, China*

† These authors contributed equally to this work.

Open Access Article. Published on 11 May 2026. Downloaded on 6/1/2026 7:58:46 PM.
This article is licensed under a Creative Commons Attribution-NonCommercial 3.0 Unported Licence.

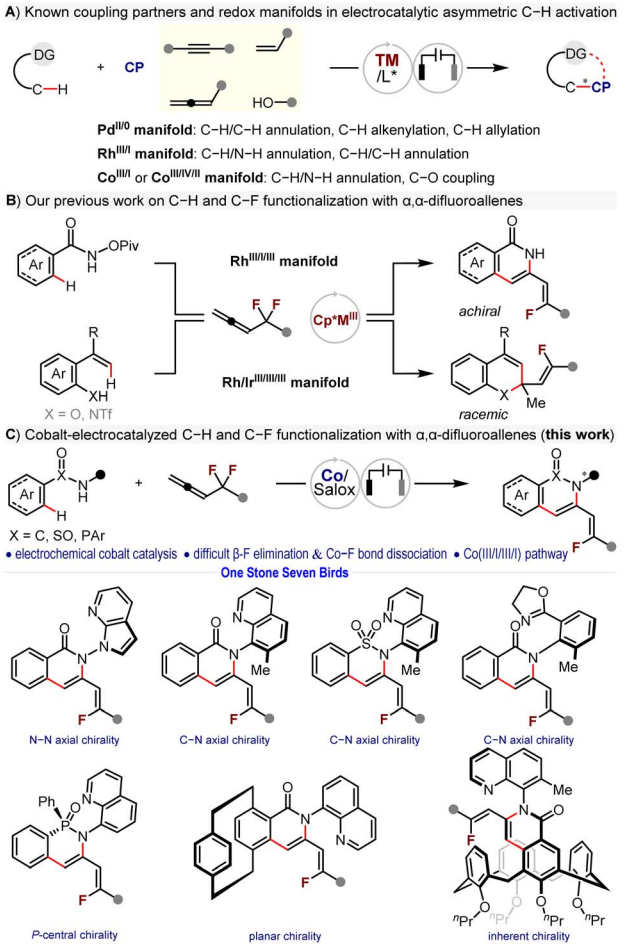

Scheme 1 Research background and motivation.

catalytic turnover; (e) electrochemical degradation of chiral Salox ligand or substrates/products. This work details a unified electrochemical cobalt/Salox-catalyzed protocol for enantioselective and stereoselective C–H and C–F functionalization of *gem*-difluoromethylene allenes (Scheme 1B). This versatile platform enables efficient access to a wide array of enantiopure (*Z*)-fluoroalkenyl azaheterocycles, integrating phosphorus-centered, N–N and C–N axial, planar, and inherent chirality. Furthermore, combined experimental and computational mechanistic studies reveal an unprecedent Co(III/I/III/I) catalytic pathway, distinct from those of analogous Rh- and Ir-catalyzed systems.[41,42]

Results and discussion

Method development

We initiated our proof-of-concept study by coupling oxidation-sensitive *N*-(7-azaindole)benzamide **1aa** with *gem*-difluoromethylene allene **2a** in an undivided cell equipped with a graphite felt (GF) anode and a platinum cathode (Table 1). Encouragingly, the electrochemical conditions previously established[32] for alkyne annulation successfully mediated the desired tandem C–H and C–F functionalization, affording isoquinolinone **3** in a promising 43% yield with 38% enantiomeric excess (ee). The molecular structure of compound **3** was unambiguously determined by X-ray crystallographic analysis, which revealed the (R_a)-configuration around N–N axis and (*Z*)-configuration within the fluoroalkenyl moiety. Subsequent optimization revealed that NaOPiv·H_2O served as an effective base and supporting electrolyte. While 1 equivalent sharply enhanced enantioselectivity at the expense of yield, increasing the loading to 2 equivalents improved the overall efficiency. The reaction yield was further increased by conducting the reaction under an air atmosphere (entry 4). The cobalt-to-Salox ratio had

Table 1 Reaction development[a]

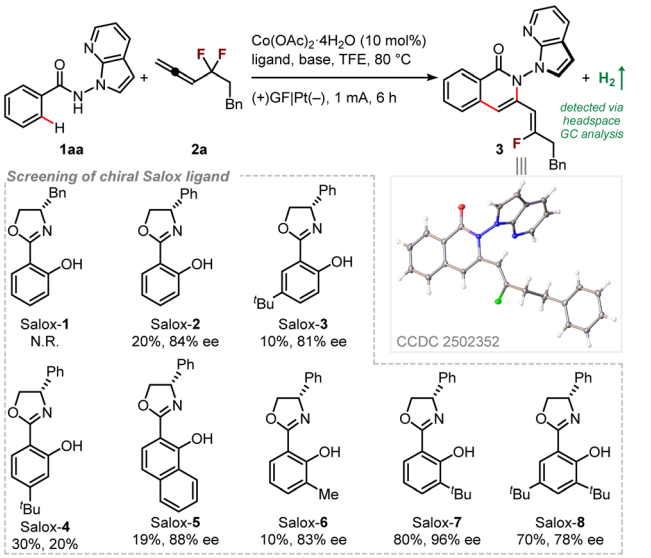

#	Ligand (mol%)	Base (equiv.)	Air/O_2	3, % Yield	ee
1	Salox-7 (20)	—	O_2	43	38
2	Salox-7 (20)	NaOPiv·H_2O (1)	O_2	14	79
3	Salox-7 (20)	NaOPiv·H_2O (2)	O_2	47	86
4	Salox-7 (20)	NaOPiv·H_2O (2)	Air	70	96
5	Salox-7 (15)	NaOPiv·H_2O (2)	Air	80	96
6	Salox-7 (10)	NaOPiv·H_2O (2)	Air	60	96
Further variation from optimal condition (entry 5, condition A)					
7	Salox-**1**–**7**		As above		
8	C as anode		20		91
9	GF as cathode		21		90
10	^{t}BuOH		31		91
11	2 mA		37		98
12	5 h		70		95
13	7 h		72		96
14	No electricity		10		75
15	No $Co(OAc)_2·4H_2O$		<1		—

[a] Conditions: **1aa** (0.08 mmol), **2a** (0.096 mmol), $Co(OAc)_2·4H_2O$ (10 mol%), ligand, base, TFE (2 mL), undivided cell with graphite felt (GF) anode (10 mm × 20 mm × 2 mm) and platinum plate (Pt) cathode (10 mm × 20 mm × 0.3 mm), 1 mA, 80 °C, 6 h. Isolated yields. Enantiomeric excess (ee) determined by HPLC with a chiral stationary phase.

© 2026 The Author(s). Published by the Royal Society of Chemistry

Open Access Article. Published on 11 May 2026. Downloaded on 6/1/2026 7:58:46 PM. This article is licensed under a Creative Commons Attribution-NonCommercial 3.0 Unported Licence.

minimal influence on reaction performance, with an optimum at 1 : 1.5. Consistent with our previous work,[32] the catalyst performance was extremely sensitive to ligand design. Only Salox-7 and Salox-**8**, which feature a bulky *ortho-tert*-butyl group on the phenol ring, showed moderate-to-good reactivity and enantioselectivity (entry 7). Alternative electrode materials gave much lower yields (entries 8 and 9). This might be rationalized by: (a) large surface area of the GF anode for cobalt contact, and (b) favorable dihydrogen evolution on the Pt surface, which was detected *via* headspace gas chromatography (GC) analysis. 2,2,2-Trifluoroethanol (TFE) was identified as the optimal solvent, likely due to its dual role in enhancing the solubility of the cobalt salt and acting as a proton shuttle (entry 10). Reaction efficacy diminished at higher current densities, suggesting possible electrochemical decomposition of the substrate or product (entry 11). Both shorter and prolonged reaction times resulted in slightly diminished yields with comparable enantioselectivity (entries 12 and 13). This observation implies that product **3** undergoes decomposition under the current electrochemical conditions. To verify this hypothesis, we resubjected enantiopure **3** to the optimal condition; no erosion of enantioselectivity was observed, but significant decomposition of **3** occurred (Section 4.8 in SI). These findings further underscore the inherent difficulty of employing benzamide **1aa** in electrochemical transformations. Control experiments verified that both the cobalt catalyst and an electrical current are essential for this tandem net-oxidation reaction (entries 14 and 15). This electro-oxidative transformation proceeds with a good current efficiency of 57%, underscoring the sustainability of the overall method.

Reaction scope

With the optimized protocols in hand, we sought to evaluate the generality of this electrocatalytic enantioselective C–H/C–F functionalization (Scheme 2). In general, a set of electronically and sterically varied benzamides proceeded smooth tandem C–H and C–F functionalization with *gem*-difluoromethylene allenes, affording the corresponding products (**3–20**) in moderate-to-good yields with excellent enantioselectivity and specific stereochemistry. This protocol tolerates diverse functional groups, including chloro (**4**), methoxy (**5**), thioether (**6**), ester (**7**), keto (**8**), cyano (**9**), nitro (**10**), and trifluoromethyl (**11**), which provides opportunities for streamlined diversification. Notably, 3-substituted benzamide underwent selective coupling in the less-hindered position (**12**). Heterocyclic (**14**) and alkenyl amides (**15**) were suitable partners. Our electrochemical protocol was also successfully applied to benzamides bearing a C2- or C3-functionalized azaindole moiety (**16**, **17**). In addition to forming N–N atropisomers, the electrochemical protocol was extended to construct C–N axially chiral compounds. This was achieved by coupling *gem*-difluoromethylene allenes with

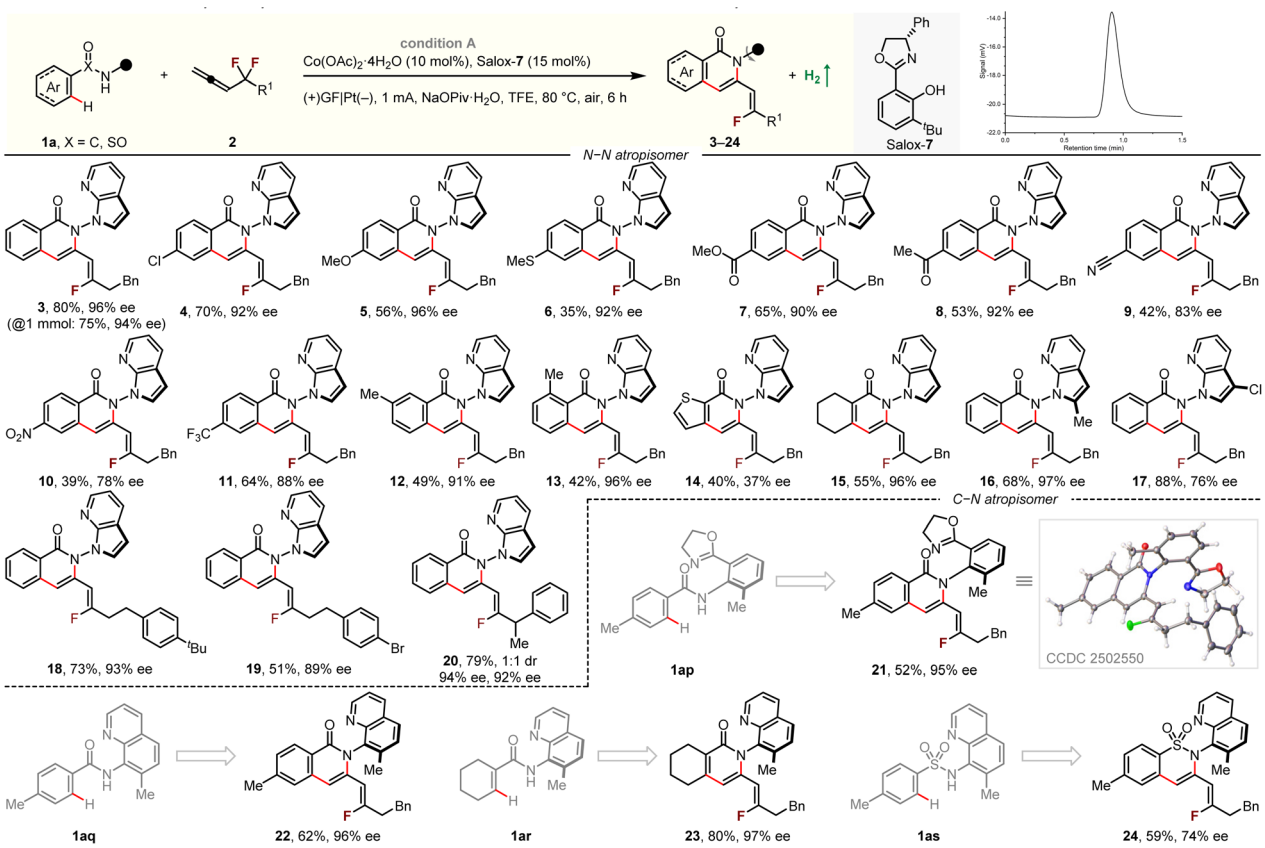

[a]Condition A: **1a** (0.08 mmol), **2** (0.096 mmol), $Co(OAc)_2{\cdot}4H_2O$ (10 mol%), Salox-**7** (15 mol%), $NaOPiv{\cdot}H_2O$ (2 equiv.), TFE (2 mL), undivided cell with GF (10 mm × 20 mm × 2 mm) and Pt cathode (10 mm × 20 mm × 0.3 mm), constant current of 1 mA (ca. 2.8 $F.mol^{-1}$), 80 °C, 6 h under air. Isolated yields. Enantiomeric excess (ee) determined by HPLC with a chiral stationary phase.

Scheme 2 Electrocatalytic asymmetric C–H/C–F functionalization to access axially chiral molecules.[a]

Open Access Article. Published on 11 May 2026. Downloaded on 6/1/2026 7:58:46 PM.
This article is licensed under a Creative Commons Attribution-NonCommercial 3.0 Unported Licence.

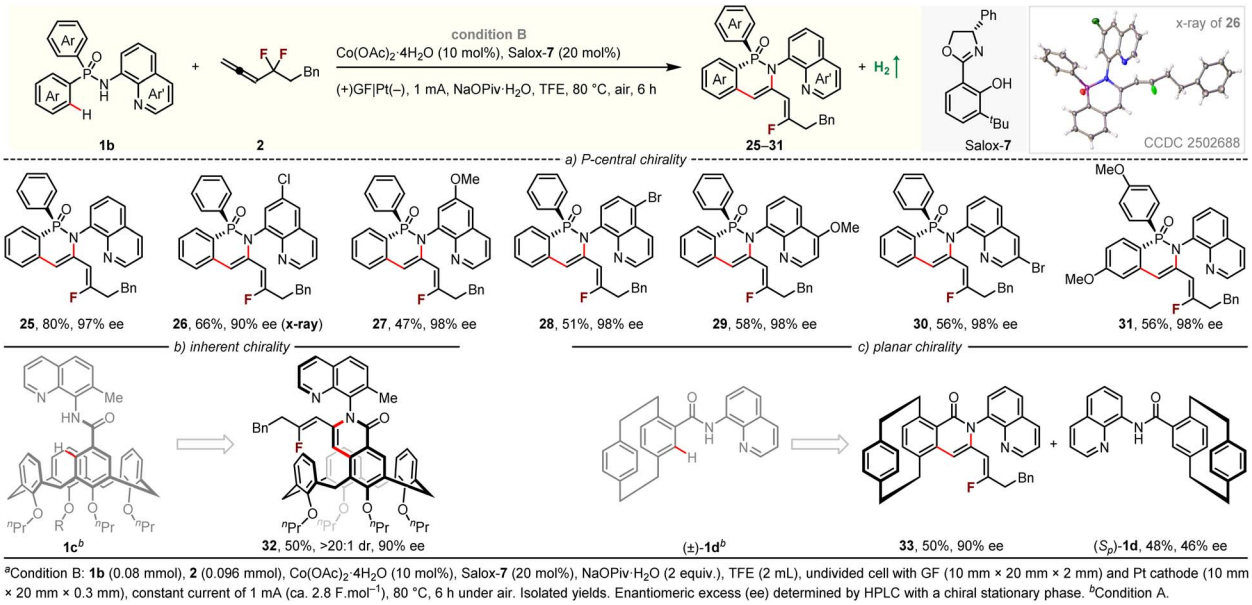

[a]Condition B: **1b** (0.08 mmol), **2** (0.096 mmol), $Co(OAc)_2{\cdot}4H_2O$ (10 mol%), Salox-**7** (20 mol%), $NaOPiv{\cdot}H_2O$ (2 equiv.), TFE (2 mL), undivided cell with GF (10 mm × 20 mm × 2 mm) and Pt cathode (10 mm × 20 mm × 0.3 mm), constant current of 1 mA (ca. 2.8 $F.mol^{-1}$), 80 °C, 6 h under air. Isolated yields. Enantiomeric excess (ee) determined by HPLC with a chiral stationary phase. [b]Condition A.

Scheme 3 Electrocatalytic asymmetric C–H/C–F functionalization to access *P*-centre, inherently, and planar chiral molecules.[a]

benzamides (**21–23**) and sulfonamides (**24**) derived from 8-aminoquinoline or 2-oxazoline aniline.

We next applied this asymmetric electrolysis to the desymmetrization of phosphinamides under only minimally modified conditions. A suite of diarylphosphinamides underwent enantioselective C–H and C–F functionalization with *gem*-difluoromethylene allene, furnishing products **25–31** in good yields with excellent enantioselectivity (Scheme 3a). X-ray crystallographic analysis of **26** unambiguously confirmed the (*R*)-configuration at the phosphine center and the (*Z*)-configuration of the fluoroalkenyl moiety. This electrocatalytic C–H/C–F functionalization was further extended to construct inherently and planar chiral molecules—valuable skeletons in asymmetric catalysis,[44,45] medicinal chemistry,[46,47] and materials science (Scheme 3b and c).[48,49] For instance, coupling calix[4]arene with *gem*-difluoromethylene allene afforded product **32**, bearing both inherent and axial chirality, in 50% yield with 90% ee and >20 : 1 dr. Kinetic resolution of racemic [2.2]paracyclophane (PCP) using *gem*-difluoromethylene allene delivered the fluorinated heterocyclic PCP derivative **33** in 50% yield and 90% ee, with recovery of enantiopure substrate (S_p)-**1d** in good yield and moderate enantiopurity. Taking together, these transformations underscore the robustness and synthetic versatility of our cobalt/Salox catalysis platform for enantioselective C–H/C–F functionalization.

Experimental mechanistic investigations

To gain insight on this electrocatalytic C–H/C–F functionalization, we performed a series of mechanistic investigations (Scheme 4). Negligible H/D scrambling was observed in the presence of D_2O, both with and without *gem*-difluoromethylene allene **2a**, pointing toward an irreversible C–H metalation step (Scheme 4A). Kinetic isotope experiments revealed a primary KIE value of 1.11 (Scheme 4B), which suggests that C–H bond cleavage is likely not involved in the rate-determining step—a conclusion consistent with our density functional theory (DFT) calculations. An intermolecular competition experiment between benzamides containing electron-rich and electron-deficient aromatic rings showed a preference for electron-deficient substrates (Scheme 4C). This finding implies a base-assisted concerted metalation deprotonation (CMD) pathway operating for C–H activation, followed by the formation of a stable C–Co bond. In support of this, the cyclometalated Co(III) species Co-I was isolated and characterized. This intermediate was stabilized by the neutral ligand 4-methoxypyridine and synthesized by treating **1aa** with an equimolar amount of $Co(OAc)_2{\cdot}4H_2O$ and Salox-**2** (Scheme 4E). This complex Co-I was found to be catalytically competent, affording product **3** in 45% yield and 88% ee, thereby strongly supporting its role as a key intermediate in the catalytic cycle. The use of either monofluoroallene **2f** or allenone **2g** as coupling partner gave unsatisfactory results, underscoring the essential role of *gem*-difluoromethylene functionality in achieving high reactivity and enantiocontrol (Scheme 4D). To probe the electrochemical landscape of the reaction, cyclic voltammetry (CV) was performed (all potentials *vs.* Ag/AgCl, Scheme 4F). Benzamide **1aa** displayed an irreversible oxidation peak at +0.78 V (curve b), confirming its susceptibility to anodic oxidation. While a mixture of $Co(OAc)_2{\cdot}4H_2O$ and $NaOPiv{\cdot}H_2O$ in TFE remained electrochemically silent across the scanned range, the introduction of Salox-**7** produced a reversible redox couple with an oxidation potential of +0.84 V (curve d/e). This value is notably anodically shifted relative to the oxidation of unbound Salox-**7** (+0.73 V, curve c). This comparison demonstrates that *in situ* complexation of Salox-**7** to the Co(II) centre not only protects the ligand from irreversible oxidative decay but also facilitates the Co(II)/Co(III) redox process.

© 2026 The Author(s). Published by the Royal Society of Chemistry

Open Access Article. Published on 11 May 2026. Downloaded on 6/1/2026 7:58:46 PM.
This article is licensed under a Creative Commons Attribution-NonCommercial 3.0 Unported Licence.

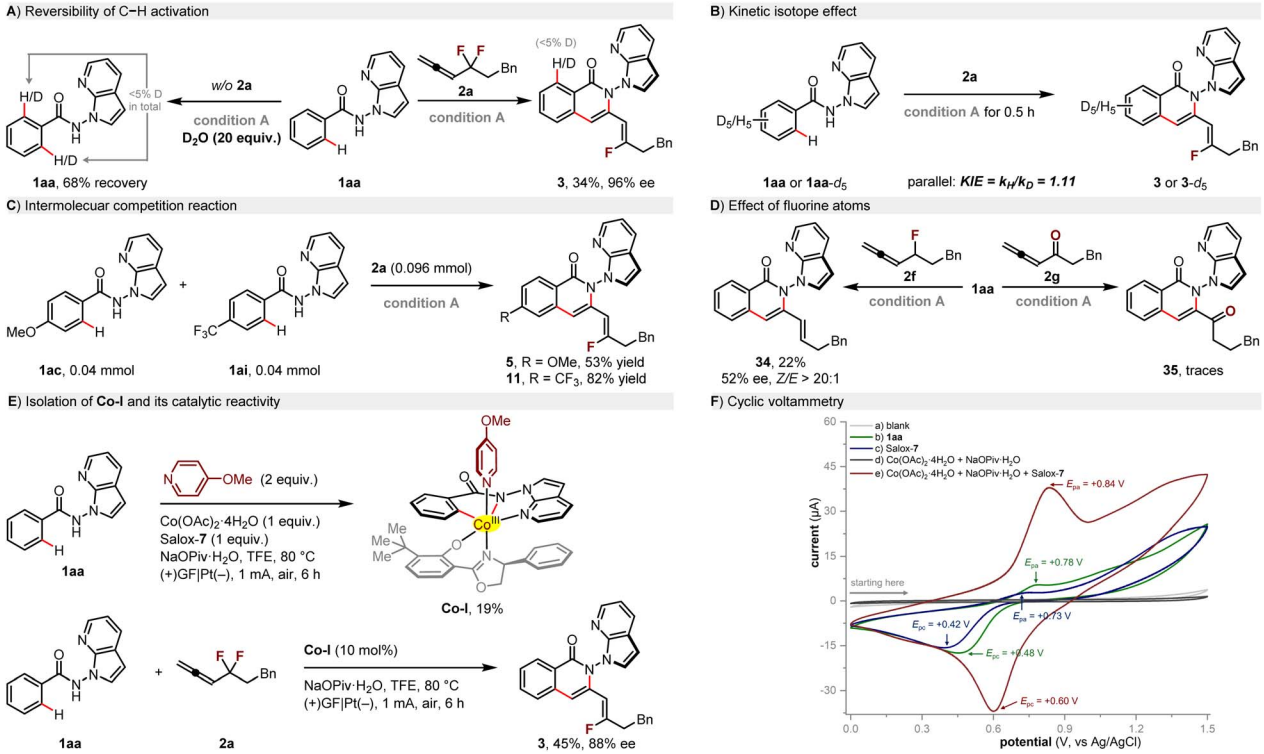

Scheme 4 Mechanistic insights.

Computational mechanistic studies

To understand the rationale behind the regio-, enantio-, and stereoselectivity in this electrocatalytic C–H and C–F functionalization, we conducted DFT calculations using Gaussian 16 at the B3LYP level in the reaction solvent (TFE). The Gibbs free energy profile of the most favorable pathway is depicted in Fig. 1A, with its spin-state evolution highlighted (a full comparison of alternative pathways is provided in SI). Initially, we examined the formation of the diastereoselective, chiral-at-cobalt complex **INT-0**, generated by C–H cyclometallation of benzamide **1aa**. Consistent with literature precedents, the cobalt center preferentially adopts the meridional, pseudo-octahedral geometry [*mer*-(S_L)-ΔCo], which is stabilized by 6.3 kcal mol^{-1} over the ΛCo isomer in the singlet state (Fig. 1B). Subsequently, coordination and migratory insertion of *gem*-difluoroallene **2a** proceeds *via* intermediate **INT-1**. This allene 1,2-insertion features a spin-crossover event (*i.e.*, ^{3}**INT-1** → ^{1}**INT-1** → ^{1}**TS-1** → ^{1}**INT-2** → ^{3}**INT-2**) and proceeds with a low free energy barrier of 21.5 kcal mol^{-1} (from ^{3}**INT-0** to ^{1}**TS-1**). Afterwards, the reaction proceeds exclusively through the spin-triplet state. In the C–N reductive elimination, the triplet transition state ^{3}**TS-2** is more favorable than its singlet counterpart, ^{1}**TS-2**, both kinetically (5.3 *vs.* 31.8 kcal mol^{-1}) and thermodynamically (−24.9 *vs.* −5.9 kcal mol^{-1}). Subsequent intramolecular allylic C(sp^3)–H oxidative addition proceeds *via* a triplet transition state (^{3}**TS-3**) with a lower free energy barrier by 15.5 kcal mol^{-1} than its singlet counterpart ^{1}**TS-3**, leading to intermediate ^{3}**INT-5**. The selective β–F elimination was calculated and revealed that the product bearing a *Z*-type configuration was more favorable dynamically, which was in good agreement with our experimental results. H–F reductive elimination at the metal center requires a 21.7 kcal mol^{-1} energy barrier *via* triplet transition state ^{3}**TS-5**, leading to the Co(I) complex ^{3}**INT-7**, which is facilitated by electrochemistry to generate the active Co(III) catalyst together with product **3** and dihydrogen in the presence of HOPiv.

To elucidate the origin of enantioselectivity, we located and compared the transition states for C–N reductive elimination. The free energy of ^{3}**TS-2**$_R$ was calculated to be 4.4 kcal mol^{-1} lower than that of its diastereomer, ^{3}**TS-2**$_S$, corresponding to an enantiomeric excess of >98% (Fig. 1C). This computational result aligns well with our experimental observation of (*R*)-selective products being obtained in excellent enantioselectivity. Independent gradient model based on Hirshfeld partition (IGMH) analysis revealed that this energy difference arises because ^{3}**TS-2**$_R$ is stabilized by both C–H···O hydrogen bonding and π···π interactions. These stabilizing forces are significantly stronger than the lone C–H···π interaction present in ^{3}**TS-2**$_S$, leading to a lower energy barrier for the pathway involving ^{3}**TS-2**$_R$.

Based on experimental and computational evidence alongside literature precedent,[32] we proposed a plausible mechanism for the electrochemical cobalt-catalyzed enantioselective C–H/C–F functionalization (Scheme 5). The cycle is initiated begins with the single-electron oxidation of the cobalt(II) salt by the anode or air in the presence of Salox-7 and NaOPiv·H$_2$O, forming the active chiral octahedral Co(III) species, **Cat.** Ligand exchange with benzamide **1aa** followed by base-assisted N–H and C–H activation generates a five-membered cobaltacycle

© 2026 The Author(s). Published by the Royal Society of Chemistry

Open Access Article. Published on 11 May 2026. Downloaded on 6/1/2026 7:58:46 PM.
This article is licensed under a Creative Commons Attribution-NonCommercial 3.0 Unported Licence.

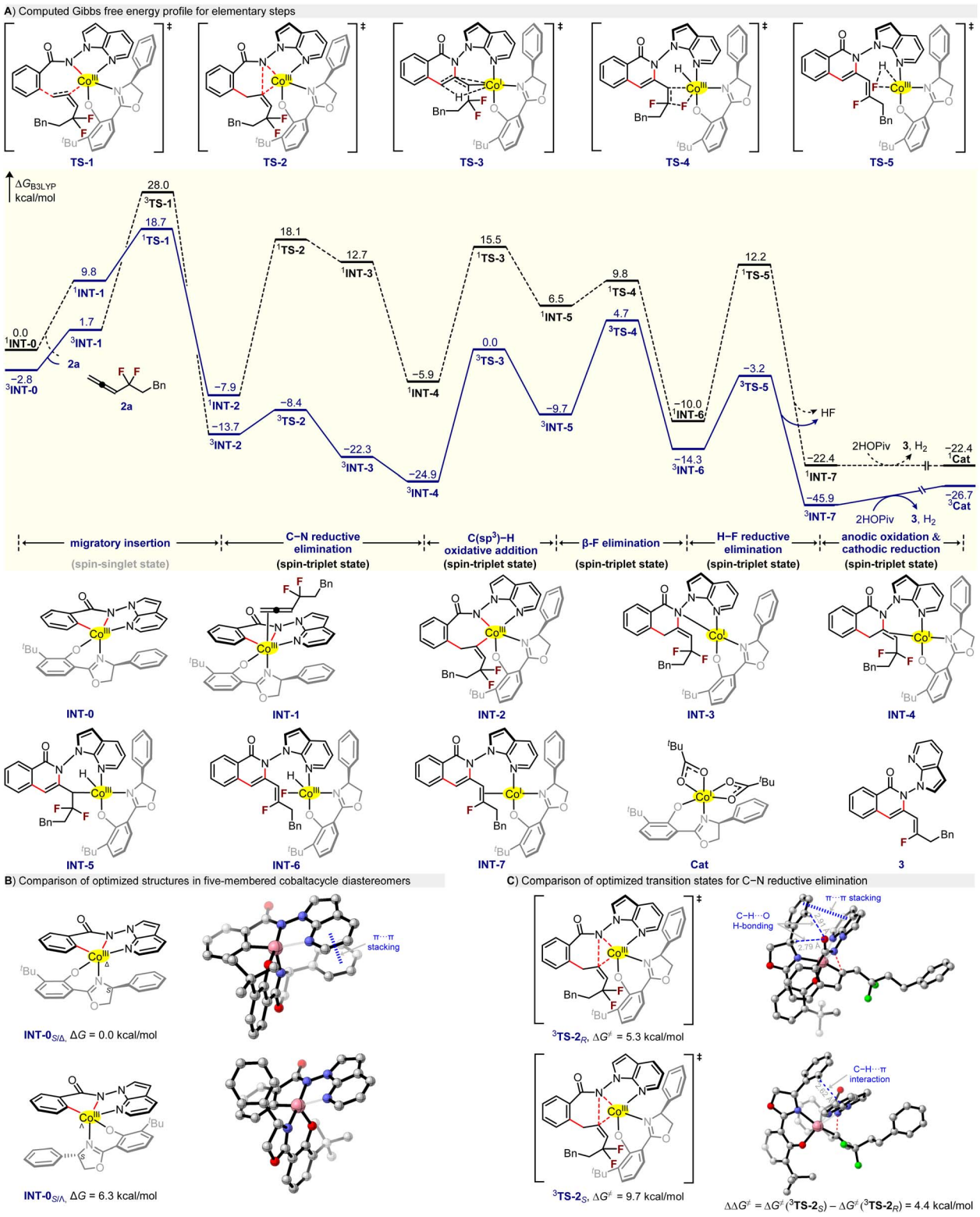

Fig. 1 DFT calculations.

INT-0. This intermediate coordinates to *gem*-difluoromethylene allene **2a**, and undergoes migratory 1,2-insertion to yield the seven-membered cobaltacycle **INT-2**. A C–N reductive elimination furnishes a Co(I) intermediate, **INT-4**, which then undergoes an intramolecular allylic C(sp^3)–H oxidative addition to form **INT-5**. Subsequent stereoselective β-F elimination and reductive elimination produces Co(I) species **INT-7**. Finally, anodic oxidation of **INT-7** releases product **3** and regenerates

© 2026 The Author(s). Published by the Royal Society of Chemistry

Open Access Article. Published on 11 May 2026. Downloaded on 6/1/2026 7:58:46 PM. This article is licensed under a Creative Commons Attribution-NonCommercial 3.0 Unported Licence.

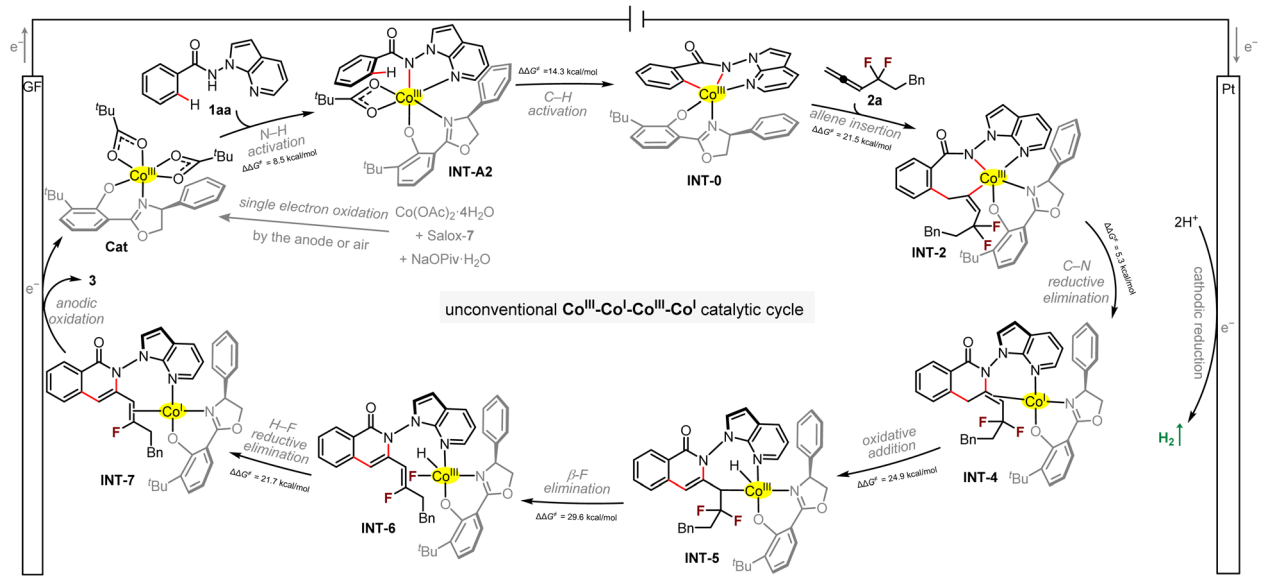

Scheme 5 Proposed mechanism.

the active Co(III) catalyst. Concurrently, protons are reduced at the cathode to evolve dihydrogen.

Conclusions

In summary, we have established a general cobalt electrocatalysis platform for enantioselective and stereoselective C–H and C–F functionalization with *gem*-difluoromethylene allenes. This approach provides efficient access to diverse enantioenriched (*Z*)-fluoroalkenyl *N*-heterocyclic frameworks containing phosphorus stereocenters, C–N and N–N axial chirality, planar chirality, and inherent chirality. This work expands the reaction paradigms of asymmetric cobalt electrocatalysis, and is poised to inspire further methodological advances and applications in synthetic and medicinal chemistry.

Author contributions

J. C.: data curation, formal analysis, investigation, validation, writing – original draft; X. G.: data curation, formal analysis, investigation, validation, writing – review & editing; C. W.: data curation, formal analysis, investigation, validation; Y. L.: data curation, formal analysis, investigation, validation; X. T.: investigation, validation; L. L.: investigation, validation; S. Q.: investigation, validation; M. Y.: investigation, validation; Q. L.: investigation, validation; W. W.: investigation, validation; L. M.: investigation, validation; M. W.: formal analysis, funding acquisition, project administration, resources, validation, writing – review & editing; S.-Y. L.: resources, writing – review & editing; Y. H.: resources, writing – review & editing; X. Z.: resources, writing – review & editing; S.W.: writing – review & editing; Z. Zhou: funding acquisition, resources, writing – review & editing; H. G.: funding acquisition, resources, writing – review & editing; W. Y.: formal analysis, funding acquisition, project administration, resources, supervision, validation, writing – review & editing; Z. Zeng: conceptualization, data curation, formal analysis, funding acquisition, investigation, project administration, resources, supervision, validation, writing – original draft, writing – review & editing.

Conflicts of interest

There are no conflicts to declare.

Data availability

CCDC 2502352, 2502550 and 2502688 contain the supplementary crystallographic data for this paper.[50a–c]

The authors confirm that all the data supporting the findings of this study are available within the article and its supplementary information (SI). Supplementary information: experimental procedures, compound characterization, and copies of NMR spectra and HPLC traces. See DOI: https://doi.org/10.1039/d6sc02228f.

Acknowledgements

We acknowledge the financial support from National Natural Science Foundation of China (No. 22201051, 82273795, 42407581), Guangdong Basic and Applied Basic Research Foundation (No. 2024A1515030179, 2024A1515010260), and Plan on Enhancing Scientific Research at GMU.

Notes and references

1 M. Yan, Y. Kawamata and P. S. Baran, *Chem. Rev.*, 2017, **117**, 13230–13319.
2 X. Chang, Q. Zhang and C. Guo, *Angew. Chem., Int. Ed.*, 2020, **59**, 12612–12622.

Open Access Article. Published on 11 May 2026. Downloaded on 6/1/2026 7:58:46 PM. This article is licensed under a Creative Commons Attribution-NonCommercial 3.0 Unported Licence.

3 L. F. T. Novaes, J. Liu, Y. Shen, L. Lu, J. M. Meinhardt and S. Lin, *Chem. Soc. Rev.*, 2021, **50**, 7941–8002.
4 D. Cantillo, *Chem. Commun.*, 2022, **58**, 619–628.
5 N. E. S. Tay, D. Lehnherr and T. Rovis, *Chem. Rev.*, 2022, **122**, 2487–2649.
6 C. A. Malapit, M. B. Prater, J. R. Cabrera-Pardo, M. Li, T. D. Pham, T. P. McFadden, S. Blank and S. D. Minteer, *Chem. Rev.*, 2022, **122**, 3180–3218.
7 K.-J. Jiao, Z.-H. Wang, C. Ma, H.-L. Liu, B. Cheng and T.-S. Mei, *Chem Catal.*, 2022, **2**, 3019–3047.
8 J. Rein, S. B. Zacate, K. Mao and S. Lin, *Chem. Soc. Rev.*, 2023, **52**, 8106–8125.
9 D. Lehnherr and L. Chen, *Org. Process Res. Dev.*, 2024, **28**, 338–366.
10 G. Laudadio, *Chimia*, 2025, **79**, 417–423.
11 Y. Wang, S. Dana, H. Long, Y. Xu, Y. Li, N. Kaplaneris and L. Ackermann, *Chem. Rev.*, 2023, **123**, 11269–11335.
12 J. F. Goebel, Z. Zeng and L. J. Gooßen, *Synthesis*, 2022, **54**, 565–569.
13 Z. Zeng, J. F. Goebel, X. Liu and L. J. Gooßen, *ACS Catal.*, 2021, **11**, 6626–6632.
14 S. Qin, M. Yang, M. Xu, Z.-H. Peng, J. Cai, S. Wang, H. Gao, Z. Zhou, A. S. K. Hashmi, W. Yi and Z. Zeng, *Nat. Commun.*, 2024, **15**, 7428.
15 U. Dhawa, C. Tian, T. Wdowik, J. C. A. Oliveira, J. Hao and L. Ackermann, *Angew. Chem., Int. Ed.*, 2020, **59**, 13451–13457.
16 U. Dhawa, T. Wdowik, X. Hou, B. Yuan, J. C. A. Oliveira and L. Ackermann, *Chem. Sci.*, 2021, **12**, 14182–14188.
17 J. Frey, X. Hou and L. Ackermann, *Chem. Sci.*, 2022, **13**, 2729–2734.
18 X. Hou, S. Li, J. Frey, X. Hong and L. Ackermann, *Chem*, 2024, **10**, 2283–2294.
19 W. Wei, A. Scheremetjew and L. Ackermann, *Chem. Sci.*, 2022, **13**, 2783–2788.
20 Y.-Q. Huang, Z.-J. Wu, L. Zhu, Q. Gu, X. Lu, S.-L. You and T.-S. Mei, *CCS Chem.*, 2022, **4**, 3181–3189.
21 G. Zhou, T. Zhou, A. Jiang, P. Qian, J. Li, B. Jiang, Z. Chen and B. Shi, *Angew. Chem., Int. Ed.*, 2024, **63**, e202319871.
22 Z.-H. Peng, P. Huang, A. Li, M. Yang, Z. Li, Y. Li, S. Qin, J. Cai, S. Wang, Z. Zhou, W. Yi, H. Gao and Z. Zeng, *ACS Catal.*, 2025, **15**, 1422–1430.
23 T. Yang, Y. Zhang, Y. Dou, D. Yang and J.-L. Niu, *Sci. China Chem.*, 2026, **69**, 659–679.
24 Q.-J. Yao and B.-F. Shi, *Acc. Chem. Res.*, 2025, **58**, 971–990.
25 T. Von Münchow, S. Dana, Y. Xu, B. Yuan and L. Ackermann, *Science*, 2023, **379**, 1036–1042.
26 Q. Yao, F. Huang, J. Chen, M. Zhong and B. Shi, *Angew. Chem., Int. Ed.*, 2023, **62**, e202218533.
27 X.-J. Si, X. Zhao, J. Wang, X. Wang, Y. Zhang, D. Yang, M.-P. Song and J.-L. Niu, *Chem. Sci.*, 2023, **14**, 7291–7303.
28 T. Liu, W. Zhang, C. Xu, Z. Xu, D. Song, W. Qian, G. Lu, C.-J. Zhang, W. Zhong and F. Ling, *Green Chem.*, 2023, **25**, 3606–3614.
29 Y. Lin, T. Von Münchow and L. Ackermann, *ACS Catal.*, 2023, **13**, 9713–9723.
30 T. Li, L. Shi, X. Wang, C. Yang, D. Yang, M.-P. Song and J.-L. Niu, *Nat. Commun.*, 2023, **14**, 5271.
31 X. Wang, X.-J. Si, Y. Sun, Z. Wei, M. Xu, D. Yang, L. Shi, M.-P. Song and J.-L. Niu, *Org. Lett.*, 2023, **25**, 6240–6245.
32 J. Cai, L. Li, C. Wang, S. Qin, Y. Li, S.-Y. Liao, S. Wang, H. Gao, Z. Zhou, Y. Huang, W. Yi and Z. Zeng, *Green Chem.*, 2024, **26**, 11524–11530.
33 Y. Zhang, S.-L. Liu, T. Li, M. Xu, Q. Wang, D. Yang, M.-P. Song and J.-L. Niu, *ACS Catal.*, 2024, **14**, 1–9.
34 Y. Sun, T. Yang, Q. Wang, L. Shi, M.-P. Song and J.-L. Niu, *Org. Lett.*, 2024, **26**, 5063–5068.
35 T. Von Münchow, Y. Liu, R. Parmar, S. E. Peters, S. Trienes and L. Ackermann, *Angew. Chem., Int. Ed.*, 2024, **63**, e202405423.
36 P. Qian, G. Zhou, J. Hu, B. Wang, A. Jiang, T. Zhou, W. Yuan, Q. Yao, J. Chen, K. Kong and B. Shi, *Angew. Chem., Int. Ed.*, 2024, **63**, e202412459.
37 X. Xia, C. Zheng, Y. Hang, J. Guo, T. Liu, D. Song, Z. Chen, W. Zhong and F. Ling, *Green Chem.*, 2024, **26**, 8323–8329.
38 L. Zhang, C. Yang, X. Wang, T. Yang, D. Yang, Y. Dou and J.-L. Niu, *Green Chem.*, 2024, **26**, 10232–10239.
39 F. Huang, M. Teng, H. Qiu, Q. Yao and B. Shi, *Angew. Chem., Int. Ed.*, 2025, **64**, e202506465.
40 G. Zhou, J. Chen, Q. Yao, F. Huang, Z. Wang and B. Shi, *Angew. Chem., Int. Ed.*, 2023, **62**, e202302964.
41 Z. Zhou, K. Chen, Y. Wang, X. Zhong, S. Lin, H. Gao and W. Yi, *Chin. Chem. Lett.*, 2023, **34**, 107849.
42 Z. Lin, Y. Cai, J. Ye, K. Chen, J. Zheng, L. Zhou, Z. Zhou and W. Yi, *Adv. Synth. Catal.*, 2025, **367**, e202401110.
43 Z. Zeng, H. Xu, H. Gao, Z. Zhou and W. Yi, *Coord. Chem. Rev.*, 2025, **522**, 216244.
44 G. E. Arnott, *Chem. Eur. J.*, 2018, **24**, 1744–1754.
45 M.-W. Chen, B. Wu, Z. Liu and Y.-G. Zhou, *Acc. Chem. Res.*, 2023, **56**, 2096–2109.
46 K. Schlotter, F. Boeckler, H. Hübner and P. Gmeiner, *J. Med. Chem.*, 2006, **49**, 3628–3635.
47 S. B. Nimse and T. Kim, *Chem. Soc. Rev.*, 2013, **42**, 366–386.
48 Y. Morisaki, M. Gon, T. Sasamori, N. Tokitoh and Y. Chujo, *J. Am. Chem. Soc.*, 2014, **136**, 3350–3353.
49 R. Kumar, A. Sharma, H. Singh, P. Suating, H. S. Kim, K. Sunwoo, I. Shim, B. C. Gibb and J. S. Kim, *Chem. Rev.*, 2019, **119**, 9657–9721.
50 (*a*) CCDC 2502352: Experimental Crystal Structure Determination, 2026, DOI: 10.5517/ccdc.csd.cc2pzx1n; (*b*) CCDC 2502550: Experimental Crystal Structure Determination, 2026, DOI: 10.5517/ccdc.csd.cc2q03f9; (*c*) CCDC 2502688: Experimental Crystal Structure Determination, 2026, DOI: 10.5517/ccdc.csd.cc2q07ww.

© 2026 The Author(s). Published by the Royal Society of Chemistry